Journal of Pharmaceutical Innovation (2023) 18:1316–1327
https://doi.org/10.1007/s12247-023-09722-9

ORIGINAL ARTICLE

Solubility Enhancement of Aripiprazole via Mesoporous Silica: Preparation, Characterization, In vitro Drug Release, and Solubility Determination

Pawan Devangan[1] · Aakash Saini[1] · Digeshwari Patel[2] · Ujwal Kolhe[1]

Accepted: 13 March 2023 / Published online: 20 March 2023

Abstract

Purpose Hollow types of mesoporous silica have been extensively used as drug delivery carriers owing to their excessive drug loading competence in the interior void cavity as well as enhancement of solubility. The main aim of this study was to improve the solubility and dissolution rate of ARPZ, a class II drug, upon incorporation into mesoporous silica (SBA-15).

Methods ARPZ was loaded in mesoporous silica using specific SBA-15 to solubilize by the wet impregnation method. The optimization was done via solubility and drug loading parameters. Characterization of the optimized formulation ARPZ-loaded SBA-15 (60%) (1.5:1 w/w) for possible molecular interaction between the ARPZ and silica was carried out by using FTIR, crystalline characteristics via PXRD, thermal analysis through DSC, and TGA, and pore size and surface area were determined by Brunauer–Emmett–Teller (nitrogen adsorption isotherm). Furthermore, an in vitro release study was examined by paddle-type dissolution apparatus (USP type II) in pH 1.2 buffer.

Results The optimized ARPZ-loaded SBA-15 (60%) showed a drug loading of 37–38% w/w. Incorporating the drug inside SBA-15 pores reduced the values of three parameters of empty SBA-15, (a) pore size from 5.21 to 4.19 nm, (b) pore volume from 0.652 to 0.178 cm^3/g, and (c) specific surface area from 622.4 to 136.7 mg^2/g. Crystalline ARPZ was converted to amorphous upon incorporation into pores of mesoporous silica. Optimized ARPZ-loaded SBA-15 (60%) exhibited more than 3 to fourfold enhancement in equilibrium solubility and dissolution after 15 min, respectively, compared to the pure ARPZ. The results showed an improvement in the solubility of ARPZ upon incorporation into pores of mesoporous silica SBA-15.

Conclusion SBA-15 was found more suitable for the solubility enhancement of the poorly water-soluble drug ARPZ.

Keywords Aripiprazole · Mesoporous silica · SBA-15 · Solubility enhancement · Schizophrenia

Introduction

Schizophrenia is a perennial psychiatric disorder [1] that affects 20 million people worldwide. This mental illness is often characterized by positive (ex: delusions, hallucinations, distorted thoughts) and negative symptoms (ex: speech destitution, confined emotional behavior, and loss of self-motivation). Various medications are available in the market for treating schizophrenia, but at present, aripiprazole (ARPZ) has gained much attention due to its potential efficacy for the treatment of both positive and negative symptoms of schizophrenia, in addition to significantly diminishing the occurrence of adverse responses. The mechanism of action of ARPZ is uncommon from those of the currently marketed typical and atypical antipsychotic drugs.

ARPZ is a second-generation neuroleptic agent which selectively binds to central dopamine D2 and serotonin (5-HT2c) receptors, appears more effective on the associated

✉ Pawan Devangan
pawandewangan011@gmail.com

Aakash Saini
aakash0766@gmail.com

Digeshwari Patel
digeshwaripatel2@gmail.com

Ujwal Kolhe
kolheud@gmail.com

[1] Department of Pharmaceutics, National Institute of Pharmaceutical Education and Research, Raebareli (NIPER-Raebareli), Bijnor-Sisendi Road, Sarojini Nagar, Near CRPF Base Camp, 226002 Lucknow, UP, India

[2] School of Pharmacy, Chouksey Engineering College, 495006 Bilaspur, Chhattisgarh, India

negative symptoms of schizophrenia, and has a lower propensity to cause extrapyramidal symptoms [2]. Furthermore, it targets the dopamine autoreceptor but has a lower affinity for D4 receptors. ARPZ is frequently used to treat schizophrenia-like mental health disorders, panic, obsessive-compulsive behavior, sleep disorder, depression, Tourette's syndrome, and manic-depressive illness [3]. However, ARPZ has poor aqueous solubility (2.8 ± 0.93 µg/mL) [4], which ultimately hampers the bioavailability of the drug, and extensively undergoes hepatic metabolism and P-glycoprotein efflux, and its acid salts as well as crystalline nature of ARPZ are the major factor for its poor solubility [5].

Poor aqueous solubility of the drug is a significant leading encounter in formulation development. Moreover, an essential characteristic of an effective and appropriate drug delivery system is that the drug should have an appropriate solubility at the absorption site. Most active pharmaceutical ingredients suffer from poor water solubility, unsatisfactory dissolution rate, low bioavailability, and less therapeutic effects [6]. This inadequate physicochemical property of APIs leads to insignificant absorption and poor bioavailability. In addition, the need for a high-strength dose to be administered leads to increased side effects. Therefore, converting the crystalline drug to its amorphous form is an attractive approach to enhance its aqueous solubility [2]. These restrictions of poor aqueous solubility and low bioavailability can be surmounted by incorporating the drug into mesoporous silica [7].

Numerous methods are reported for enhancing the solubility of poorly aqueous soluble drugs, such as particle size reduction, formulating solid dispersion, co-crystal, inclusion complex, use of surfactant, via nanoparticles, cosolvency, hydrotropy, salt formation, and physical and chemical modifications [8, 9]. Among this solubility enrichment technique, mesoporous silica has been widely employed to enhance the solubility of drugs. It has expanded concern in the pharmaceutical sector, indicating a rapid expansion of their potential uses in drug delivery, especially in oral dosage forms [10]. A new avenue for enhancing the solubility of poorly soluble drugs has been made possible by introducing inorganic porous materials as dominant drug carriers [11].

Incorporating the API into pores of mesoporous silica is one of the supreme promising strategies to enrich the solubility of poorly water-soluble API. According to the IUPAC definition, "mesoporous" refers to porous materials with 2-50 nm in diameter pores [12]. Mesoporous silica particles (MSPs) have gained much popularity for drug delivery in recent years due to their extensive several specific properties, including high surface area, high pore volume, solid skeleton, flexible inside and outside surface modification, excellent drug loading capacity, tunable particle size, high thermal, chemical and physical stability, non-toxic, biodegradability, and biocompatibility [13]. Moreover, reliant on the particle and pore size in addition to the chemistry of mesoporous silica's large external and internal surface, it can be utilized to achieve a tunable sustained or targeted release of the incorporated drugs to augment its stability via shielding from premature release and degradation [14]. Incorporating a crystalline drug into pores of mesoporous silica converts the drug into an amorphous form and enhances the solubility as well as dissolution rate of the drug. Several types of mesoporous silica have been reported for solubility enhancement of crystalline drugs such as celecoxib [15], paclitaxel [16], carbamazepine [17], fenofibrate [18], ezetimibe [19], carvedilol [20], telmisartan [21], valsartan [22], ketoprofen [23], and cyclosporine [24]. The mesoporous silica serves as a drug delivery system, allowing alteration of the pharmacological release site, improving the release rate, and enhancing bioavailability by fashioning highly soluble active substances [25].

ARPZ is used for treating schizophrenia, which belongs to BCS class II, having low solubility [26] and high permeability. Hence, there is an urgent need to develop a formulation to enhance the solubility of ARPZ. Earlier approaches to improving the solubility of ARPZ including nanocrystals [27], solid dispersion [28], cyclodextrin complexation [29], self-nano-emulsifying drug delivery system [30], and silicosan particles [31] were reported. However, to our knowledge, no study was carried out to enhance the solubility of ARPZ by incorporating it into mesoporous silica.

The present study aimed to investigate the solubility enhancement of ARPZ via mesoporous silica particles of SBA-15 (Santa Barbara Amorphous-15). MSPs enable higher drug loading and a simple processing technique compared to earlier efforts for the solubility enhancement of ARPZ. ARPZ was loaded in SBA-15 by the wetness impregnation method. The drug was loaded at different ARPZ to SBA-15 ratios, such as 1:1, 1.5:1, and 2.34:1. Moreover, based on the drug content and equilibrium solubility of drug-loaded MSPs, further optimization was carried out. ARPZ to SBA-15 at a feed ratio of 1.5:1 exhibited higher solubility and maximum drug content. Hence, this ratio was further characterized for morphology (SEM), thermal analysis (DSC and TGA), powder XRD, and FTIR spectroscopy. The pore characterization of the sample was determined by the nitrogen adsorption method, and the in vitro drug release studies were performed in pH 1.2 HCl buffer. So, SBA-15 was more suitable for solubility enhancement of poorly soluble drugs such as ARPZ.

Materials and Methods

Materials

Aripiprazole was purchased from KV biotech (Lucknow, India), and SBA-15 (8 nm), dichloromethane (DCM), methanol, ethanol (99%), sodium hydroxide, and hydrochloric

acid were obtained from Merck Specialties (Mumbai, India). Potassium chloride was purchased from Hi-Media Laboratories (Mumbai, India). MiliQ double distilled water was used for the experiments. All other solvents and chemicals were of analytical reagent grade.

Formulation of ARPZ-Loaded MSPs

Earlier reported wet impregnation method [32] was used to load ARPZ in mesoporous silica particles. SBA-15 was used as an ordered MSP. Briefly, the ARPZ was dissolved in 15 mL dichloromethane, followed by the addition of MSPs in 1:1 (50 % w/w), 1.5:1 (60 % w/w), and 2.34:1 (70 % w/w) ratio of ARPZ to MSPs. These mixtures were stirred for 24 h using a magnetic stirrer. The mixtures were centrifuged at 4000 rpm for 10 min to obtain ARPZ-loaded SBA-15 sediment. The sediments were dried overnight at ambient temperature to remove traces of the solvents.

Drug Loading Quantification

ARPZ content of ARPZ-loaded MSPs was determined by suspending 5 mg of the sample in 5 mL of ethanol. The suspensions were vortexed for 30 min, followed by centrifugation at 4000 rpm for 10 min for separated mesoporous silica residue. The concentration of ARPZ was determined by analyzing the supernatant by UV–spectrophotometer at 255 nm in triplicate after suitable dilutions with ethanol. The percentage drug loading was calculated by using the following formula,

$$\% \text{ Drug loading} = \frac{\text{Amount of drug in formulation}}{\text{Amount of formulation taken}} \times 100$$

Equilibrium Solubility

The equilibrium solubility of ARPZ and ARPZ-loaded SBA-15 were performed in pH 1.2 HCl buffer solutions. Excess amounts of samples were added in 5 mL of the buffer solution in a 25-mL conical flask in triplicate. The solutions were kept for shaking on a mechanical shaker for 24 h. Afterward, solutions were centrifuged at 4000 rpm for 10 min. The drug content in the supernatant solution was determined by a UV-visible spectrophotometer at 249 nm after appropriate dilutions with pH 1.2 HCl buffer solutions.

Morphology

The surface morphology of pure ARPZ, SBA-15, and the optimized ARPZ-loaded SBA-15 (60%) was studied by scanning electron microscope (SEM, JSM 6490, JEOL, Japan). The samples were positioned on the stubs with double-sided adhesive tape and were gold-plated beforehand to capture the pictures. The electron microscope was operated at an acceleration voltage of 15 kV. The working distance was maintained at 12-14 mm. The samples were viewed at a magnification of ×500, ×2500, ×10,000, and ×15,000 with a secondary electron detector and a backscattered electron detector.

Powder X-ray Diffraction (PXRD) Analysis

Powder XRD was performed to identify the presence of crystalline and amorphous nature of samples. Powder X-ray diffractograms of ARPZ, SBA-15, ARPZ-loaded SBA-15 (60%), and a physical mixture of ARPZ and SBA-15 were collected using a powder X-ray diffractometer (X'PERT Powder, PANalytical; Netherland) equipped with a Cu Kα target. The X-rays were generated at 30 mA and 40 kV. Data were obtained in the range from 3 to 50° (diffraction angle 2θ) at a step size of 0.013° and a dwell time of 23.97 s per step.

Differential Scanning Calorimetry (DSC)

The thermal analysis of the sample was carried out by differential scanning calorimetry (DSC 25, TA, USA). The instrument was calibrated using indium and an empty aluminum pan as a reference. About 5-10 mg of pure ARPZ, SBA-15, ARPZ-loaded SBA-15 (60%), and a physical mixture of ARPZ and SBA-15 were accurately weighed into an aluminum tzero pan, and it was sealed with the help of a tzero lid and crimped shut. The sample was heated from 25 to 250 °C at a heating rate of 10 °C/min under a nitrogen purge of 50 mL/min.

Thermogravimetric Analysis (TGA)

The thermal behavior of ARPZ, SBA-15, physical mixture of ARPZ and SBA-15, and ARPZ-loaded SBA-15 (60%) was analyzed through thermogravimetric analysis. It was performed using a TGA/DSC-1 instrument (Mettler Toledo, USA) at 10 °C/min heating rate under a nitrogen purge of 40 mL/min.

Fourier Transform Infrared Spectroscopy Analysis (FTIR)

Functional group analysis of ARPZ, SBA-15, physical mixture of ARPZ and SBA-15, and optimized ARPZ-loaded SBA-15 (60%) were performed using an FTIR spectrometer (Bruker Alpha, USA). The FTIR spectra were obtained in absorbance mode over the spectral region of 400–4000 cm^{-1}.

Nitrogen Adsorption Studies

The pore characteristics of the SBA-15 and the optimized ARPZ-loaded SBA-15 (60%) were evaluated by the nitrogen adsorption-desorption isotherm using a surface area and pore size analysis (Autosorb-1, Quantachrome, Japan) at −196 °C. The instrument was calibrated by injecting a known quantity of nitrogen. Before analysis, the weighed samples were degassed to remove moisture and contamination. SBA-15 and the optimized ARPZ-loaded SBA-15 (60%) were subjected to 150 °C for 24 h. The pore size and the surface area were determined using the Brunauer–Emmett–Teller (BET) equation and the Barrett–Joyner–Halenda (BJH) procedure from the adsorption branches of the isotherms.

In vitro Drug Release Study

In vitro, drug release studies of pure ARPZ and ARPZ-loaded SBA-15 were carried out in triplicate using the USP type II paddle dissolution test apparatus (DS 8000, Labindia, Mumbai) in pH 1.2 HCl buffer. The ARPZ and the ARPZ-loaded SBA-15 equivalent to 5 mg ARPZ were added to 250 mL of pH 1.2 HCl buffer solution at 37 ± 0.5°C at 75 rpm. An aliquot of a 5-mL sample was withdrawn from the dissolution vessel at 2.5, 5, 10, 15, 30, 45, and 60 min and filtered through a 0.22-µm filter paper. The withdrawn 5 mL medium was replaced immediately with a fresh 5-mL dissolution medium to keep the total volume constant. The amount of drug in the filtrate was determined by a UV-visible spectrophotometer at 249 nm.

Results and Discussions

Drug Loading

The amount of ARPZ in MSPs (1:1, 1.5:1, and 2.34:1) was determined via a UV-visible spectrophotometer as well as TGA, and the results are given in Table 1. One of the main primary intentions of this study was to achieve a high-loading ability of ARPZ molecules. The maximum drug loading, 37.1 % w/w, was found in a 1.5:1 ratio of ARPZ to SBA-15. The actual drug loading in the ARPZ-loaded SBA-15 increased with a drug concentration, but there was a plateau above 1:1 and 2.34:1 ratio of ARPZ to SBA-15, which might be due to the saturation of all the pores of MSPs by the drug.

Table 1 Theoretical and practical drug loading into mesoporous silica particles

Mesoporous silica	Drug: SBA-15 ratio (wt%)	TDL (%)	PDL (%)
SBA-15	50/50	50	29.7 ± 5.6
	60/40	60	37.1 ± 1.4
	70/30	70	34.7 ± 1.5

TDL theoretical drug loading, *PDL* practical drug loading

Equilibrium Solubility

The result of equilibrium solubility studies of the ARPZ and ARPZ-loaded SBA-15 mesoporous silica in ratios of 1:1 (50% w/w ARPZ), 1.5:1 (60% w/w ARPZ), and 2.34:1 (70% w/w ARPZ) is given in Fig. 1. There was a marked enhancement in the equilibrium solubility of ARPZ-loaded SBA-15 compared to that of the pure ARPZ drug. A similar solubility enhancement in drug-loaded mesoporous silica particles was reported for carbamazepine upon incorporation into MSPs [17]. The solubility enhancement was attributed to converting crystalline drugs to amorphous forms.

SEM Analysis

The SEM images of the pure ARPZ, SBA-15, and ARPZ-loaded SBA-15 (60%) are shown in Fig. 2 [(A and B) SBA-15, (C and D) ARPZ-loaded SBA-15 (60%), and (E) pure ARPZ]. SEM images (A and B) of SBA-15 revealed that SBA-15 was rod-like, aggregated into the wheat-like long fibrous macrostructure packed. This category of syllable structure has been recognized to have similar long-range channels alongside the hexagonal mesostructures, a typical morphology of this SBA-15 mesoporous silica [17]. The explained morphology was reported by Xu et al. [33]. The SEM image of pure ARPZ (E) disclosed that APRZ exists as aggregated crystalline. Moreover, SEM photomicrographs of ARPZ-loaded SBA-15 (60%) (C and D) revealed the change in the arrangement of the wheat-like macrostructure into irregularly spaced rod-like units upon drug loading into mesoporous silica. Similar outcomes were also observed in the case of ibuprofen-loaded SBA-15 (50:50, w/w) [34].

PXRD Analysis

The PXRD diffractograms of ARPZ, SBA-15, physical mixture of ARPZ and SBA-15, and ARPZ-loaded SBA-15 (60%) are given in Fig. 3.

ARPZ X-ray diffractogram (Figure 3A) exhibited two sharp peaks at 20.4° and 22.1° beyond numerous secondary peaks indicating its crystalline nature. It was also consistent with the results of the previous literature [35]. Due to the crystalline nature of ARPZ, the physical mixture of ARPZ and SBA-15 (D) also showed crystal diffraction peaks in the diffraction pattern. In the SBA-15 (C) diffractogram, some sharp peak at nearly 19° and 25° was observed, but ARPZ-loaded SBA-15 (60%) (B) did not exhibit any sharp peak

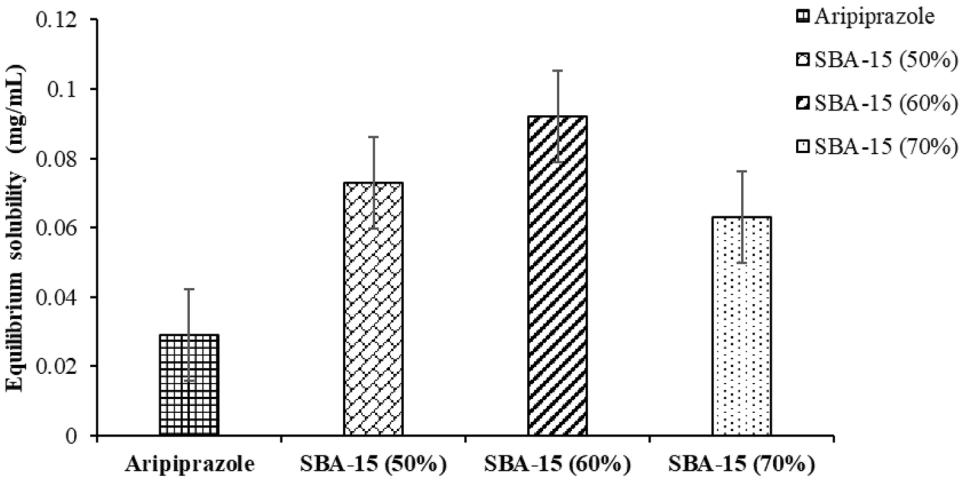

Fig. 1 Equilibrium solubility of the ARPZ and ARPZ-loaded SBA-15 at various ratios

in the diffractograms, representing their amorphous nature. Therefore, PXRD analysis revealed the conversion of the crystalline nature of ARPZ into amorphous after incorporation into SBA-15 pores. Similar results of amorphization of a crystalline drug upon incorporation into mesoporous silica particles for telmisartan and celecoxib were reported earlier [15, 36]. However, in all these cases, intensities of peaks were absent in the PXRD pattern of drug-loaded mesoporous carriers, which might be due to the reduced crystallinity of the drug after the adsorption of the drug on the mesoporous carriers.

Differential Scanning Calorimetry (DSC)

The DSC thermograms of pure ARPZ, SBA-15, physical mixture of ARPZ and SBA-15, and ARPZ-loaded SBA-15 (60%) are given in Fig. 4.

The thermogram of pure ARPZ, SBA-15, physical mixture of ARPZ and SBA-15, and ARPZ-loaded SBA-15 (60%) helps to determine the crystallinity and amorphous form. As shown in Fig. 4B, the sharp endothermic melting peak of ARPZ was observed at 140.59 °C, which is the melting point of the ARPZ drug, and the exothermic peak was observed at 95 °C which attributed to the crystallization temperature and indicating an exothermic reaction caused by crystallization. However, crystallization is an exothermic process, so heat is released to the surroundings. A very low-intensity endothermic peak was also observed at nearly 140.59 °C in ARPZ-loaded SBA-15 (`%) in Fig. 4C because ARPZ was incorporated in pores of mesoporous silica in a noncrystalline state. However, in the case of ARPZ-loaded SBA-15 (60%), a very weak crystalline peak (low-intensity endothermic peak) could still originate, demonstrating the presence of some traces of crystalline ARPZ drugs or a tiny amount of free ARPZ crystalline drug.

Similar results were also reported in the case of carvedilol crystalline and carvedilol-loaded hollow mesoporous silica nanoparticles [37]. In this case, the DSC thermogram shows quite a little crystallinity, but PXRD data show an utterly amorphous nature; there may be numerous possibilities, such as decomposition of ARPZ, solid–solid transformation, and a slight presence of small fraction crystals and phase separation of ARPZ and SBA-15. One other prospect may occur, a minimal number of little crystallites scattered within the amorphous matrix, and the sensitivity of PXRD cannot be high enough to confirm crystallinity even though the DSC thermogram showed quite a little crystallization peak. The presence of the melting point of ARPZ in the physical mixture of ARPZ and SBA-15 (60%) was also confirmed (Fig. 4D). The DSC curve of SBA-15 (Fig. 4A) presents an endothermic transition that occurs near 100 °C that was assigned due to dehydration or unbound water molecules.

Thermogravimetric Analysis (TGA)

The TGA graph of ARPZ, SBA-15, physical mixture of ARPZ and SBA-15, and ARPZ-loaded SBA-15 (60%) are illustrated in Fig. 5.

The total amount of loaded ARPZ drug inside the mesoporous silica can be quantified using TGA. In the TGA measurement, the drug desorbs after decomposition, which is detected as a temperature-dependent weight reduction [38]. Quantifying the mesopore-loaded drug fraction in mesoporous materials is more complex than just quantifying the total drug content of the sample [39]. As shown in Fig. 5, the ARPZ loading fraction in SBA-15 was estimated from the weight loss ratio between 100 and 500 °C to the total initial weight. Furthermore, 5.5 % and 1.4 % weight loss were observed in SBA-15 and ARPZ-loaded SBA-15 (60%), respectively. The weight loss below 100 °C in all the samples was not considered, which might be due to the evaporation of the moisture entrapped inside the pores after reaching 100 °C [40]. A sudden weight reduction of the ARPZ (drug) was observed at around

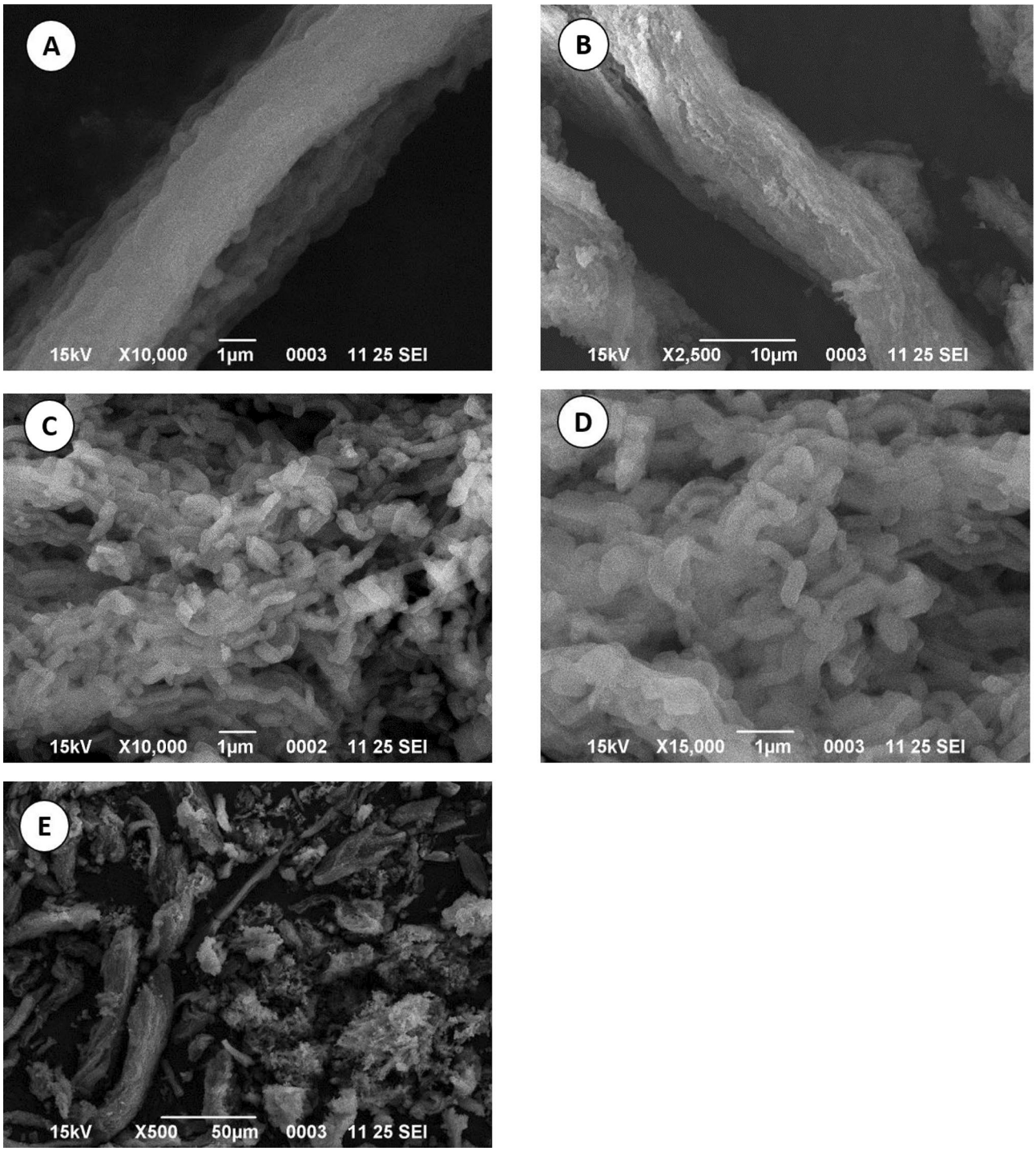

Fig. 2 SEM photomicrographs of **A** and **B** SBA-15, **C** and **D** ARPZ-loaded SBA-15 (60%), and **E** pure ARPZ; the wheat-like macrostructure of rod-like SBA-15 has been disrupted upon the incorporation of ARPZ

260°C, and almost more quantity of the drug was degraded at about 400 °C while the SBA-15 amount was constant up to 500 °C. The loss in the weight of ARPZ-loaded SBA-15 (60%) indicated the amount of ARPZ loaded in the SBA-15. The weight loss due to the drug present in ARPZ-loaded SBA-15 (60%) was found to be 38.8 % w\w. This result agreed with the drug loading value of 37.1 % w/w, determined using UV spectroscopic analysis [41]. A similar weight loss trend in TGA for ketoprofen-loaded MSN was reported earlier [42].

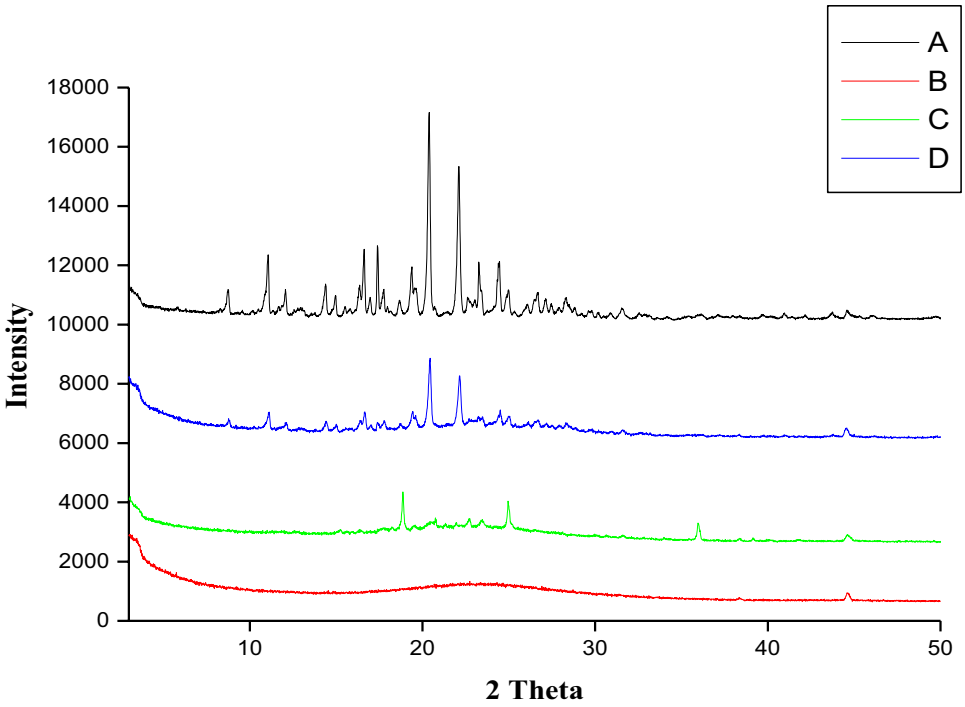

Fig. 3 PXRD patterns of **A** ARPZ, **B** ARPZ-loaded SBA-15 (60%), **C** SBA-15, and **D** physical mixture of ARPZ and SBA-15

FTIR Analysis

The FTIR spectra of ARPZ, SBA-15, physical mixture of ARPZ and SBA-15, and ARPZ-loaded SBA-15 (60%) are given in Fig. 5.

FTIR studies were performed to determine the molecular interactions between the ARPZ and SBA-15. The lack of a crystal structure may lead to changes in bonding between chemical groups. Two intense absorption peaks at 1061.14 and 809.20 cm^{-1} were attributed to the stretching vibrations of the -Si-O-Si- framework in SBA-15, shown in Fig. 6B [18, 43, 44]. FTIR spectrum of plain ARPZ (Fig. 6A) exhibits characteristic stretching frequencies at 3182, 2939, 1519, 1669, and 1272 cm^{-1} for N-H, aliphatic C-H, aromatic C=C,

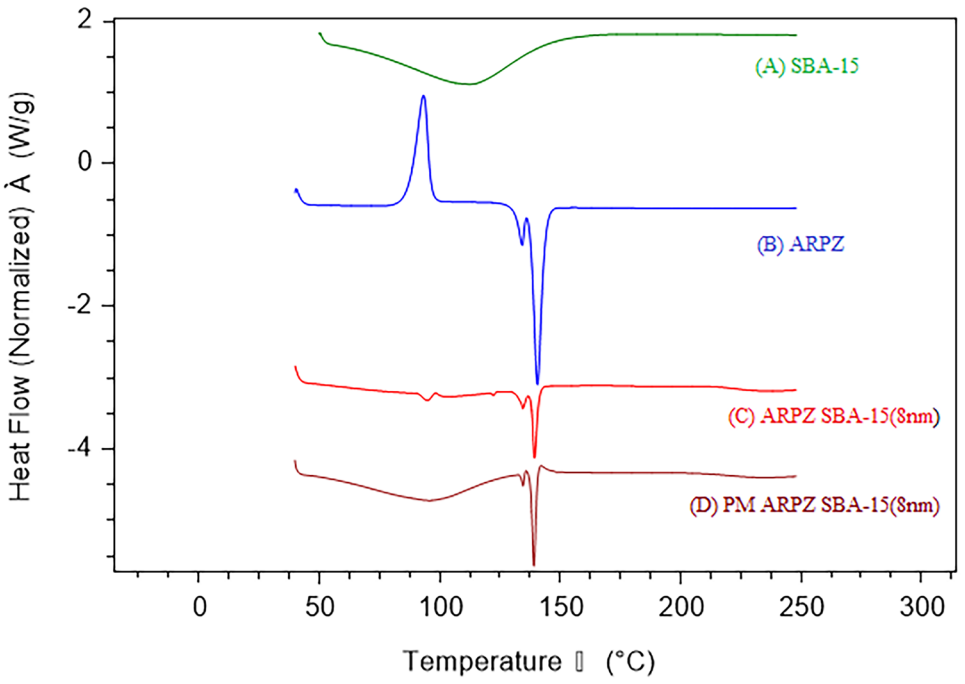

Fig. 4 DSC thermogram of **A** SBA-15, **B** ARPZ, **C** ARPZ-loaded SBA-15 (60%), and **D** physical mixture of ARPZ and SBA-15; a very weak intensity peak in the ARPZ-loaded SBA-15 (60%) was observed due to presence of some traces of crystalline ARPZ drugs, crystalline ARPZ amorphization upon loading into SBA-15

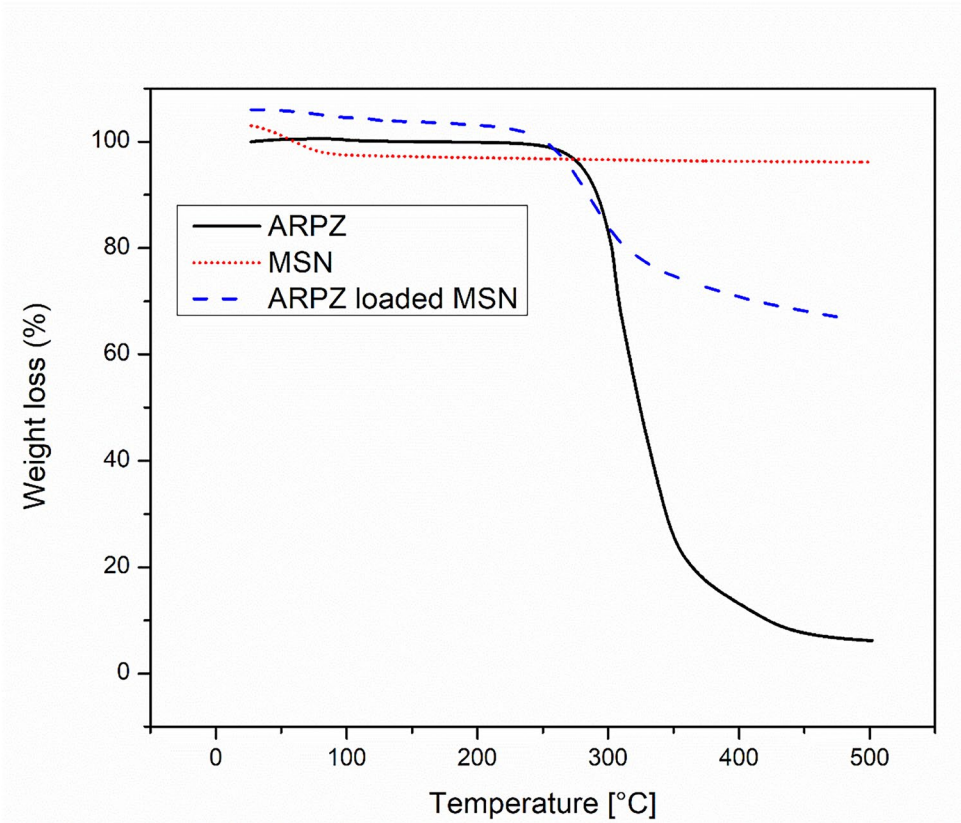

Fig. 5 TGA of **A** ARPZ (continuous black line), **B** SBA-15 (red small dotted line), and **C** ARPZ-loaded SBA-15 (60%) (blue dashed line); the weight loss at 260 °C corresponds to drug degradation, which has been taken as clue for determination of drug loading since SBA-15 does not show degradation up to 500 °C

and aromatic C-O, respectively [29]. In ARPZ-loaded SBA-15 (60%) (Fig. 6D), only two peaks, i.e., at 1061.14 and 809.20 cm^{-1}, were observed due to asymmetric and symmetric stretching vibrations of the -Si-O-Si- (Siloxane) and Si–O bending vibrations to the outer surface framework of SBA-15 [43, 44]. Still, in the physical mixture of ARPZ and SBA-15 (Fig. 6C), both ARPZ and SBA-15 characteristic peaks were observed. The absence of ARPZ distinct peaks in ARPZ-loaded SBA-15 (60%) indicated the entrapment of the drug within the mesoporous silica pores. A similar result was reported in FTIR studies of fenofibrate and fenofibrate-loaded hexagonal mesoporous silica, wherein the characteristic peaks of fenofibrate were absent of fenofibrate-loaded hexagonal mesoporous silica [45].

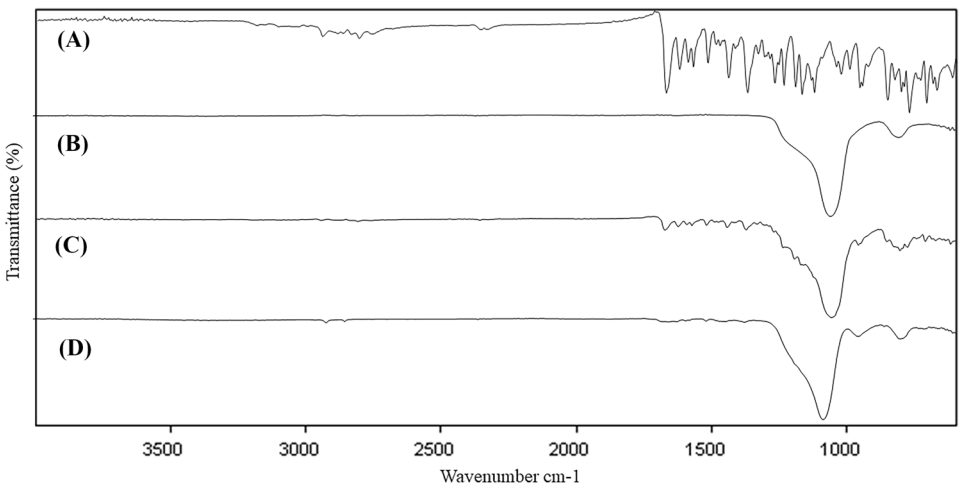

Fig. 6 FTIR spectra of **A** ARPZ, **B** SBA-15, **C** physical mixture of ARPZ and SBA-15, **D** ARPZ-loaded SBA-15 (60%); the absence of characteristic absorption peaks of ARPZ in the ARPZ-loaded SBA-15 sample indicates incorporation of the ARPZ drug inside the pores of MSPs

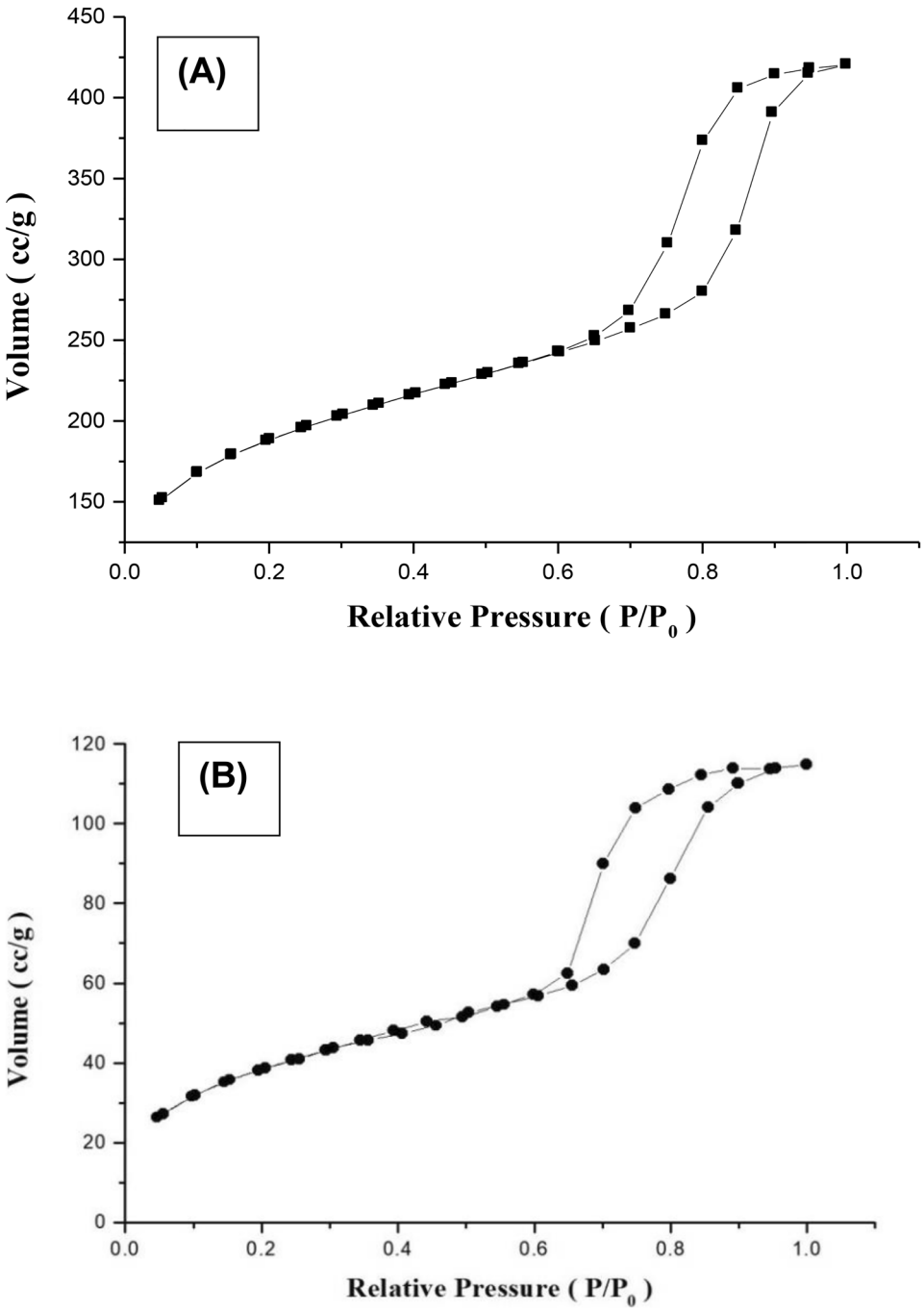

Fig. 7 Nitrogen adsorption/desorption isotherm of **A** SBA-15 and **B** ARPZ-loaded SBA-15 (60%); this is a typical isotherm IV type for mesoporous materials, and there is a decrease in pore volume upon drug ARPZ loading into SBA-15 which indicates incorporation of the drug inside the pores

Nitrogen Adsorption Isotherm

Nitrogen adsorption isotherms of SBA-15 and ARPZ-loaded SBA-15 (60%) are given in Fig. 7.

The nitrogen adsorption/desorption isotherms of ARPZ and ARPZ-loaded SBA-15 (60%) (Fig. 7A, B) exhibited a typical type IV isotherm according to IUPAC classification [46], a characteristic isotherm of mesoporous materials as shown by an inflection of capillary condensation at P/P_0 value of about 0.6. The values for the BET-specific surface area (S_{BET}), the total pore volume (Vt), and the BJH pore

Table 2 Characterization of SBA-15 before and after drug loading

Sample name	S_{BET} (m^2/g)	*Pore volume Vt* (cm^3/g)	W_{BJH} (nm)	Drug loading (%) TGA	Drug loading (%) UV
SBA-15	622.4	0.652	5.21	-	-
ARPZ-loaded SBA-15 (60%)	136.7	0.178	4.19	38.8	37.1

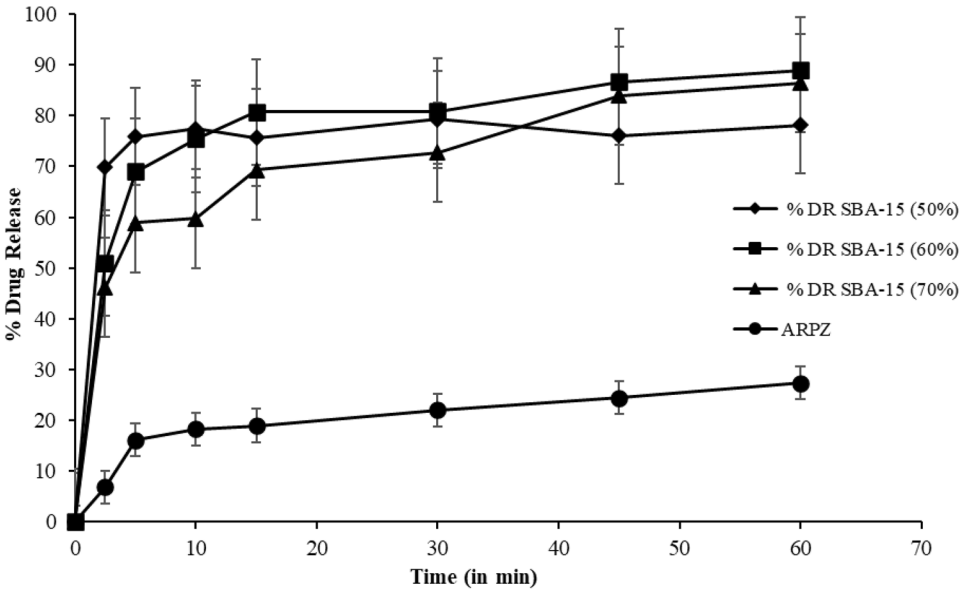

Fig. 8 Cumulative drug release of pure ARPZ and ARPZ-loaded SBA-15 MSPs; the drug release from ARPZ-loaded SBA-15 has been increased drastically compared to that from the ARPZ per se due to amorphization of the drug

diameter (W_{BJH}) are given in Table 2. Higher S_{BET} and *Vt* values of SBA-15 indicated its potential application as a host in bonding or storing more drug molecules [47]. Furthermore, these results revealed that S_{BET}, *Vt*, and W_{BJH} were reduced in the case of ARPZ-loaded SBA-15 (60%). In the ARPZ-loaded SBA-15 (60%) sample, a drastic reduction in S_{BET}, *Vt*, and W_{BJH} were observed, as shown in Table 2. This reduction can be attributed to the loading of ARPZ inside the pores of SBA-15. Similar results of decrease in S_{BET}, *Vt*, and W_{BJH} were reported earlier for felodipine, insulin, and ibuprofen-loaded mesoporous silica particles as compared to unloaded mesoporous silica particles [48–50].

In vitro Drug Release

The drug release profiles of pure ARPZ and ARPZ-loaded SBA-15 are given in Fig. 8.

In vitro, drug release studies were executed to prove the chief function of mesoporous silica to enhance the solubility parameter of ARPZ. The dissolution rate improvement of ARPZ-loaded SBA-15 might be due to primarily recognized to the pore channels of the SBA-15 altering the crystalline structure of ARPZ to an amorphous state, which is known to improve the solubility of ARPZ. However, solid-state characterization further confirmed the amorphization of the ARPZ-loaded SBA-15. Although aripiprazole is poorly water-soluble, it has pH-dependent solubility and slightly higher solubility under strongly acidic media than basic and neutral media. The release of the ARPZ from SBA-15 involves three steps, i.e., (a) entry of dissolution medium into mesoporous silica pores due to osmotic pressure, (b) dissolution of the drug, and (c) diffusional transport of dissolved drug into the dissolution medium [51].

The enhancement of the drug release from ARPZ-loaded SBA-15 is due to the following: (a) conversion of crystalline ARPZ to an amorphous state [21, 36, 13] and (b) higher BET-specific surface area of the ARPZ-loaded SBA-15 mesoporous silica particles [17]. The dissolution rate of ARPZ from MSPs was faster than that from pure ARPZ. However, 50 % w/w ARPZ-loaded SBA-15 exhibited a burst release of about 76 % within 5 min, and 60 % and 70 % ARPZ-loaded SBA-15 showed 69 % and 59 % burst release, respectively, followed by prolonged release up to 1 h. A similar burst release pattern followed by an extended-release was reported by Dodrio et al. and Jesus et al. for gentamicin sulfate and efavirenz after loading into SBA-15 [52, 53]. There was a reduction in drug release from ARPZ-loaded MSPs with drug loading due to high competition of release from pores of mesoporous silica [54].

Conclusion

The solubility and dissolution rate of the poorly aqueous soluble drug ARPZ was enhanced by incorporating it into mesoporous silica using a wet impregnation method. UV spectroscopic and thermogravimetric analyses revealed 37-38% w/w drug loading into the mesoporous silica particles. Furthermore, FTIR analysis revealed the absence of characteristic peaks of the ARPZ, indicating the ARPZ (drug) incorporated inside the pores of mesoporous silica particles. However, PXRD studies showed the conversion of the ARPZ from a crystalline state to an amorphous state. The incorporation of the ARPZ inside the pores of mesoporous particles has been revealed by a reduction in pore surface area, pore volume, and pore diameter of the

empty mesoporous particles. The morphological studies using SEM exhibited disruption of the wheat-like macrostructure of rod-like mesoporous silica upon ARPZ loading. Based on the combination of all numerous characterization studies, we have verified that ARPZ can be encumbered into the internal pores of mesoporous silica. Moreover, equilibrium solubility and in vitro drug release studies revealed that the drug solubility and dissolution rate were enhanced more than 3-fold to 4-fold upon loading into mesoporous silica. These enhancements have been attributed to drug amorphization upon loading into mesoporous silica. Hence, the loading of ARPZ into SBA-15 (8 nm) mesoporous silica was found as a suitable approach for solubility enhancement.

Here, this study will support the strategy to design oral drug delivery systems for solubility improvement and dissolution rate enhancement of poorly water-soluble APIs, as well as lead to more potential applications in drug delivery systems.

Acknowledgements The authors acknowledge the Central Instrumentation Facility of NIPER, Raebareli for the characterization. AS and PD are grateful for the scholarship provided by the Department of Pharmaceuticals, Ministry of Chemicals and Fertilizers, India.

Data Availability All the data generated or analysed during this study are included in this published article.

Declarations

Conflict of Interest The authors declare no competing interests.

References

1. Tandon R, Gaebel W, Barch DM, Bustillo J, Gur RE, Heckers S, et al. Definition and description of schizophrenia in the DSM-5. Schizophr Res. 2013;150(1):3–10.
2. Zajdel P, Marciniec K, Ma A, Lenda T, Siwek A, Nowak G, et al. Antidepressant and antipsychotic activity of new quinoline- and isoquinoline-sulfonamide analogs of aripiprazole targeting serotonin 5-HT_1A/5-HT_2A/5-HT_7 and dopamine D_2/D_3 receptors. Eur J Med Chem. 2013;60:42–50.
3. Mcintyre RS, Yoon J, Jerrell MJ, Liauw SS. Aripiprazole for the maintenance treatment of bipolar disorder: a review of available evidence. Neuropsychiatr Dis Treat. 2011;7:319–23.
4. Butreddy A, Sarabu S, Bandari S, Dumpa N, Zhang F, Repka MA. Polymer-assisted aripiprazole-adipic acid cocrystals produced by hot melt extrusion techniques. Cryst Growth Des. 2020;20(7):4335–45.
5. Silki, Sinha VR. Enhancement of in vivo efficacy and oral bioavailability of aripiprazole with solid lipid nanoparticles. AAPS PharmSciTech. 2018;19(3):1264–1273.
6. Ghadi R, Dand N. BCS class IV drugs: highly notorious candidates for formulation development. J Control Release. 2017;248:71–95.
7. He Y, Liang S, Long M, Xu H. Mesoporous silica nanoparticles as potential carriers for enhanced drug solubility of paclitaxel. Mater Sci Eng C Mater Biol Appl. 2017;78:12–7.
8. Savjani KT, Gajjar AK, Savjani JK. Drug solubility : importance and enhancement techniques. ISRN Pharm. 2012;195727:1–10.
9. Danısman-Kalındemirtaş F, Karïper IA, Hepokur C, Erdem-Kuruca S. Selective cytotoxicity of paclitaxel bonded silver nanoparticle on different cancer cells. J Drug Deliv Sci Technol. 2021;61:102265.
10. Huang R, Shen Y, Guan Y, Jiang Y, Wu Y, Rahman K, et al. Mesoporous silica nanoparticles : facile surface functionalization and versatile biomedical applications in oncology. Acta Biomater. 2020;116:1–15.
11. Jafari S, Derakhshankhah H, Alaei L, Fattahi A, et al. Mesoporous silica nanoparticles for therapeutic/diagnostic applications. Biomed Pharmacother. 2019;109:1100–11.
12. Meynen V, Cool P, Vansant EF. Verified syntheses of mesoporous materials. Microporous Mesoporous Mater. 2009;125(3):170–223.
13. Zhou J, Zhu F, Li J, Wang Y. Concealed body mesoporous silica nanoparticles for orally delivering indometacin with chiral recognition function. Mater Sci Eng C Mater Biol Appl. 2018;90:314–24.
14. Soltys M, Kovacik P, Dammer O, Beranek J, Stepanek F. Effect of solvent selection on drug loading and amorphisation in mesoporous silica particles. Int J Pharm. 2019;555:19–27.
15. Laine A, Price D, Davis J, Roberts D, Hudson R, Back K, et al. Enhanced oral delivery of celecoxib via the development of a supersaturable amorphous formulation utilising mesoporous silica and co-loaded HPMCAS. Int J Pharm. 2016;512(1):118–25.
16. Jia L, Shen J, Li Z, Zhang D, Zhang Q, Duan C, et al. Successfully tailoring the pore size of mesoporous silica nanoparticles : exploitation of delivery systems for poorly water-soluble drugs. Int J Pharm. 2012;439(1–2):81–91.
17. Wang Z, Chen B, Quan G, Li F, Wu Q, Dian L, et al. Increasing the oral bioavailability of poorly water-soluble carbamazepine using immediate-release pellets supported on SBA-15 mesoporous silica. Int J Nanomedicine. 2012;7:5807–18.
18. Hong S, Shen S, Tan DCT, Ng WK, Liu X, Chia LSO, et al. High drug load, stable, manufacturable and bioavailable fenofibrate formulations in mesoporous silica: a comparison of spray drying versus solvent impregnation methods. Drug Deliv. 2016;23(1):316–27.
19. Kiekens F, Eelen S, Verheyden L, Daems T, Martens J, Mooter G. Use of ordered mesoporous silica to enhance the oral bioavailability of ezetimibe in dogs. J Pharm Sci. 2012;101(3):1136–44.
20. Zhang Y, Zhi Z, Li X, Gao J, Song Y. Carboxylated mesoporous carbon microparticles as new approach to improve the oral bioavailability of poorly water-soluble carvedilol. Int J Pharm. 2013;454(1):403–11.
21. Zhang Y, Wang J, Bai X, Jiang T, Zhang Q, Wang S. Mesoporous silica nanoparticles for increasing the oral bioavailability and permeation of poorly water soluble drugs. Mol Pharm. 2012;9(3):505–13.
22. Biswas N. Modified mesoporous silica nanoparticles for enhancing oral bioavailability and antihypertensive activity of poorly water soluble valsartan. Eur J Pharm Sci. 2017;99:152–60.
23. Abd-Elrahman AA, El Nabarawi MA, Hassan DH, Taha AA. Ketoprofen mesoporous silica nanoparticles SBA-15 hard gelatin capsules: preparation and in vitro/in vivo characterization. Drug Deliv. 2016;23(9):3387–98.
24. Dai W, Guo Y, Zhang H, Wang X, Zhang Q. Sylysia 350/Eudragit S100 solid nanomatrix as a promising system for oral delivery of cyclosporine A. Int J Pharm. 2015;478(2):718–25.
25. Bukara K, Schueller L, Rosier J, Martens MA, Daems T, Verheyden L, et al. Ordered mesoporous silica to enhance the bioavailability of poorly water-soluble drugs: proof of concept in man. Eur J Pharm Biopharm. 2016;108:220–5.
26. Braun DE, Gelbrich T, Kahlenberg V, Tessadri R, Wieser J, Griesser UJ. Stability of solvates and packing systematics of nine crystal forms of the antipsychotic drug aripiprazole. Cryst Growth Des. 2009;9(2):1054–65.
27. Al-dhubiab BE. Aripiprazole nanocrystal impregnated buccoadhesive films for schizophrenia. J Nanosci Nanotechnol. 2017;17(4):2345–52.

28. McFall H, Sarabu S, Shankar V, Bandari S, Murthy SN, Kolter K, et al. Formulation of aripiprazole-loaded pH-modulated solid dispersions via hot-melt extrusion technology: in vitro and in vivo studies. Int J Pharm. 2019;554:302–11.
29. Mihajlovic T, Kachrimanis K, Graovac A, Djuric Z, Ibric S. Improvement of aripiprazole solubility by complexation with (2-hydroxy)propyl-β-cyclodextrin using spray drying technique. AAPS PharmSciTech. 2012;13(2):623–31.
30. Sahoo SK, Suresh P, Acharya U. Formulation development and bioavailability assessment of aripiprazole by self-nanoemulsifying drug delivery systems. Asian J Pharm. 2018;12(03):1059–68.
31. Mahmoud AA, Salama AH, Shamma RN. Bioavailability enhancement of aripiprazole via silicosan particles : preparation, characterization and in vivo evaluation. AAPS PharmSciTech. 2018;8:3751–62.
32. Quan G, Pan X, Wang Z, Wu Q, Li G, Dian L, et al. Lactosaminated mesoporous silica nanoparticles for asialoglycoprotein receptor targeted anticancer drug delivery. J Nanobiotechnology. 2015;13(1):1–12.
33. Xu Y, Wang C, Zhou G, Wu Y, Chen J. Improving the controlled release of water-insoluble emodin from amino-functionalized mesoporous silica. Appl Surf Sci. 2012;258(17):6366–72.
34. Shen S, Ng WK, Chia L, Dong YC, Tan RB. Stabilized amorphous state of ibuprofen by co-spray drying with mesoporous SBA-15 to enhance dissolution properties. J Pharm Sci. 2010;99(4):1997–2007.
35. Mihai I, Laura T, Adriana S, Gabriela L, Paul V, Renata B, et al. Physicochemical characterization and molecular modeling study of host-guest systems of aripiprazole and functionalized cyclodextrins. J Therm Anal Calorim. 2020;141:1027–39.
36. Zhang Y, Zhi Z, Jiang T, Zhang J, Wang Z, Wang S. Spherical mesoporous silica nanoparticles for loading and release of the poorly water-soluble drug telmisartan. J Control Release. 2010;145(3):257–63.
37. Geng H, Zhao Y, Liu J, Cui Y, Wang Y, Zhao Q, et al. Hollow mesoporous silica as a high drug loading carrier for regulation insoluble drug release. Int J Pharm. 2016;510(1):184–94.
38. Rahmat N, Sadon N, Yusof MA. Thermogravimetric analysis (TGA) profile at different calcination conditions for synthesis of PTES-SBA-15. Am J Appl Sci. 2017;14(10):938–44.
39. Jadhav SA, Brunella V, Scalarone D, Berlier G. Poly (NIPAM-co-MPS)-grafted multimodal porous silica nanoparticles as reverse thermoresponsive drug delivery system. Asian J Pharm Sci. 2017;12(3):279–84.
40. Marzouqa DM, Zughul BM, Taha OM, Hodali AH. Effect of particle morphology and pore size on the release kinetics of ephedrine from mesoporous MCM-41 materials. J Porous Mater. 2012;19:825–33.
41. Shah PV, Rajput SJ. Facile synthesis of chitosan capped mesoporous silica nanoparticles : a pH responsive smart delivery platform for raloxifene hydrochloride. AAPS PharmSciTech. 2018;3:1344–57.
42. Abd-Elrahman AA, El Nabarawi MA, Hassan DH, Taha AA. Ketoprofen mesoporous silica nanoparticles SBA-15 hard gelatin capsules: preparation and in vitro/in vivo characterization. Drug Deliv. 2016;23:3387–98.
43. Guo X, Feng Y, Ma L, Gao D, Jing J, Yu J, et al. Phosphoryl functionalized mesoporous silica for uranium adsorption. Appl Surf Sci. 2017;402:53–60.
44. Jin Q, Qu F, Jiang J, Dong Y, Guo W, Lin H. A pH-sensitive controlled dual-drug release from meso-macroporous silica/multilayer-polyelectrolytes coated SBA-15 composites. J Sol-Gel Sci Technol. 2013;66:466–71.
45. Jadhav NV, Vavia PR. Dodecylamine template-based hexagonal mesoporous silica (HMS) as a carrier for improved oral delivery of fenofibrate. AAPS PharmSciTech. 2017;18:2764–73.
46. Alothman ZA. A review: fundamental aspects of silicate mesoporous materials. Materials (Basel). 2012;5(12):2874–902.
47. Yang P, Quan Z, Lu L, Huang S, Lin J. Luminescence functionalization of mesoporous silica with different morphologies and applications as drug delivery systems. Biomaterials. 2008;29(6):692–702.
48. Wu C, Zhao Z, Zhao Y, Hao Y, Liu Y, Liu C. Preparation of a push-pull osmotic pump of felodipine solubilized by mesoporous silica nanoparticles with a core-shell structure. Int J Pharm. 2014;475(1–2):298–305.
49. Elsayed A, Al-remawi M, Maghrabi I, Hamaidi M, Jaber N. Development of insulin loaded mesoporous silica injectable particles layered by chitosan as a controlled release delivery system. Int J Pharm. 2014;461(12):448–58.
50. Shen S, Kiong W, Chia L, Hu J, Tan RBH. Physical state and dissolution of ibuprofen formulated by co-spray drying with mesoporous silica : effect of pore and particle size. Int J Pharm. 2011;410(1–2):188–95.
51. Wang S. Ordered mesoporous materials for drug delivery. Microporous Mesoporous Mater. 2009;117(1–2):1–9.
52. Jesus RA, Rabelo AS, Figueiredo RT, Cides LC, Codentino IC, Fantini MCA, et al. Synthesis and application of the MCM-41 and SBA-15 as matrices for in vitro efavirenz release study. J Drug Deliv Sci Technol. 2016;31:153–9.
53. Doadrio AL, Sousa EMB, Doadrio JC, Pe J, et al. Mesoporous SBA-15 HPLC evaluation for controlled gentamicin drug delivery. J Control Release. 2004;97(1):125–32.
54. Ulfa M, Prasetyoko D. Infrared spectroscopic and scanning electron microscopy study of ibuprofen loading onto the molecular sieve mesoporous silica SBA-15 material. Oriental J of Chem. 2018;34(5):1–6.